# Modeling of Waveguide PIN Photodetectors Under Very High Optical Power

Joseph Harari, Frédéric Journet, Omar Rabii, Guanghai Jin, Jean Pierre Vilcot, and Didier Decoster

*Abstract*—**In this paper, the behavior under very high optical power of waveguide PIN photodetectors grown on InP substrate is simulated. The problem is solved using a pseudo-bidimensional Drift-Diffusion model which describes the electrical behavior of the device including the effects of the external circuit. The optical behavior of the device is analysed using FD 2D and 3D Beam Propagation Method. First, we present the optical behavior of the device when the illumination conditions change. Influence of device structure, spot width, spot position and injection angle on the quantum efficiency of the photodetector is so studied. Second, the whole modeling is validated using experimental results given in the literature. Three typical multimode structures which allow a high cut-off frequency as well as a good responsivity are then modeled and compared. The smaller one has a cut-off frequency of 75 GHz in small signal conditions and the main effect decreasing the microwave output signal when the optical input power increases is the carrier effect in the depletion region of the photodetector. The maximum microwave power of each photodetector is calculated in typical conditions of use.**

## I. Introduction

OPTICAL links can be an interesting way to carry high power microwave signals. Some works have already been carried out to analyse the behavior of photodetectors under high power modulated optical signals. Concerning top illuminated PIN photodiodes, theoretical [1] as well as experimental works [2]–[4] have already been reported. The maximal cut-off frequency of such devices is around 20 GHz when a high quantum efficiency (>70%) is achieved. Concerning Metal-Semiconductor-Metal photodetector on GaAs or InP substrate, theoretical works have also been made [5], [6], for frequency range around 20 GHz. It could be then interesting to analyse the behavior of photodetectors under very high optical power in the 60-GHz frequency range. In this case, the waveguide PIN photodetector is a good candidate [7]. Experimental studies have already been made [8]–[11]. Wake *et al.* [11] observed saturation effect but the effects of the device structure on this phenomenon are not known. This is why we present the modeling of such a device including the external circuit under very high optical modulated power.

Manuscript received January 5, 1995; revised April 15, 1995. This work was supported in part by the RACE2005 Modal project.

The authors are with the Institut d'Electronique et de Microélectronique du Nord, UMR CNRS 9929, DHS, Av Poincaré BP 69, 59652 Villeneuve d'Ascq cedex, France.

IEEE Log Number 9413678.

## II. Modeling

The simulated waveguide PIN photodetector (PD) is grown on InP substrate. An example of structure is given in Fig. 1. The light is injected on the side of the photodetector and the size of the optical spot must be small if we want to get a high responsivity. Generally a lensed fiber is used [7], [11], which gives a spot width in the order of some micrometers. In such conditions, Kato *et al.* [7] measured a spot width of 1.3 $\mu$m. We consider in this paper values between 1.3 and 4 $\mu$m which are much smaller than the spot width issued from a classical cleaved monomode fiber. In such a multilayered structure, the propagation of the injected light is complicated because the optical energy is redistributed during the propagation. This drove us to study precisely the propagation of the light in the photodetector with a Beam Propagation Method (BPM). Moreover, an electrical monodimensional modeling is not sufficient for this photodetector, so we used a pseudo-bidimensional model.

### A. Analysis of the Optical Behavior:

Considering a cross-sectional index profile $n(x, y, z)$ and in the paraxial limit, we must solve the scalar paraxial wave equation [12]. In the case of gaussian beam injection in the photodetector, we consider the propagation of the light from the air-semiconductor interface ($Z = 0$ $\mu$m), to the end of the waveguide PD ($Z = 12$ $\mu$m). There is no frontal reflexion of the light during the propagation inside the waveguide, so it is not necessary to use a bidirectionnal Fast Fourier Transform (FFT) BPM [13]. We used the Finite Difference (FD) scheme and realized two algorithms (3D and 2D FD BPM) whose principle is described in [14] and calculation time smaller than those of equivalent FFT BPM algorythms [14].

The 3D analysis that we made shows that there is no lateral effect ($Y$ direction) if the spot width do not exceed the rib width, so the distribution of the optical energy inside the waveguide can be calculated with a 2D algorithm. For this reason we mainly used the 2D FD BPM algorithm which is less time consuming and coupled it with the electrical model, but some results of 3D BPM will be presented in this paper.

*Monomode or Multimode Waveguide PIN Structure?:* In order to obtain a high cut-off frequency device, the low doped absorbing layer must be very thin to decrease the carrier transit time in the depletion region: the studied undoped layer thicknesses are 0.2, 0.4 and 0.6 $\mu$m. The device surface has also to be small in order to decrease the capacitance effect (we chose a rib width of 5 $\mu$m and a device length of 12 $\mu$m).

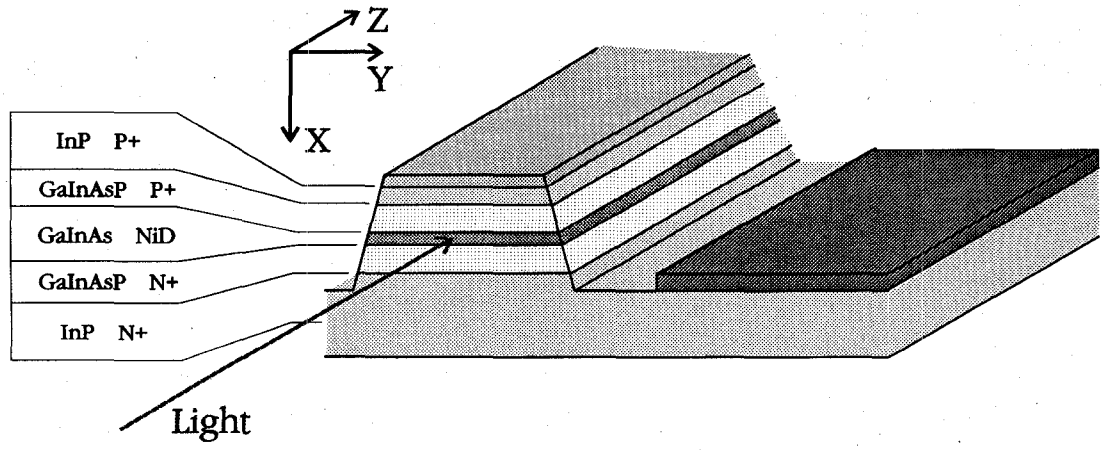


Fig. 1. Example of structure of waveguide PIN photodetector grown on InP substrate. The GaInAsP is transparent at the wavelength of injected light.

TABLE I
WAVEGUIDE PIN PD STRUCTURES INTRODUCED IN THE CALCULATION

| | structure 1 | structure 2 | structure 3 |
|---|---|---|---|
| rib width ($\mu$m) | 5 | 5 | 5 |
| length ($\mu$m) | 12 | 12 | 12 |
| InP cap layer (P+) | 0.4$\mu$m, $10^{18}$cm$^{-3}$ | 0.4$\mu$m, $10^{18}$cm$^{-3}$ | 0.4$\mu$m, $10^{18}$cm$^{-3}$ |
| GaInAsP (P+) | 0.6$\mu$m, $10^{18}$cm$^{-3}$ | 0.6$\mu$m, $10^{18}$cm$^{-3}$ | 0.6$\mu$m, $10^{18}$cm$^{-3}$ |
| GaInAs (I) | 0.2$\mu$m, $10^{15}$cm$^{-3}$ | 0.4$\mu$m, $10^{15}$cm$^{-3}$ | 0.6$\mu$m, $10^{15}$cm$^{-3}$ |
| GaInAsP (N+) | 0.6$\mu$m, $10^{18}$cm$^{-3}$ | 0.6$\mu$m, $10^{18}$cm$^{-3}$ | 0.6$\mu$m, $10^{18}$cm$^{-3}$ |
| InP (N+) | ~, $10^{18}$cm$^{-3}$ | ~, $10^{18}$cm$^{-3}$ | ~, $10^{18}$cm$^{-3}$ |

From the optical point of view, the structure can be symmetric or asymmetric, monomode or multimode and the top metallization can have a great influence on the optical behavior. In our work, we chose to simulate symmetric structures but we do not forget that the results presented by Kato *et al.* [15] and Wake *et al.* [11] demonstrated the possibility to obtain also a high quantum efficiency with assymmetric ones. The refractive indexes introduced in the calculations are from [16], [17].

The waveguide PIN structure is made multimode by growing around the GaInAs layer two transparent P+ and N+ GaInAsP layers ($\lambda_c = 1.3$ $\mu$m). This increases the thickness of the waveguide. We studied the behavior of multimode and monomode structures. A representative example follows. The distributions of the optical energy in the waveguide PIN photodetector for the two cases are presented in Fig. 2. This shows the typical behavior of each type of structure.

For the monomode structure (identical to structure 2 of Table I but the quaternary layers are replaced by InP ones), a certain part of the injected light is lossed into the InP substrate and in the InP cap layer and by this very fact not absorbed. The quantum efficiency which can be obtained with such a structure is 0.72 (0.50 if we take into account the air-semiconductor reflexion at the input of the waveguide). On the contrary, the diagrams concerning the multimode structure in Fig. 2 show that the quaternary epilayers confine the light in the GaInAs layer during propagation. The optical energy first injected in InP and GaInAsP is progressively redistributed in the absorbing layer and absorbed during propagation. This

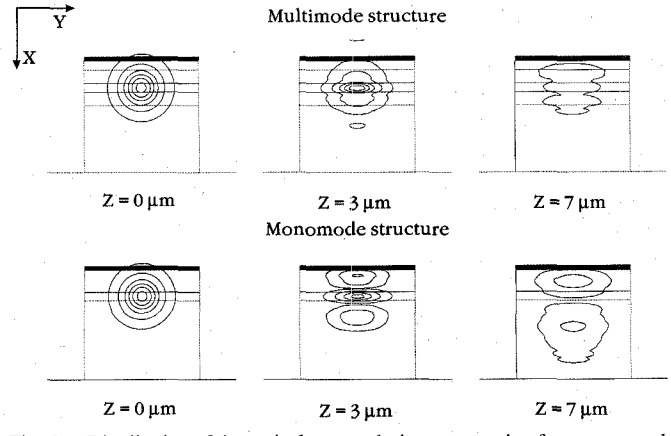


Fig. 2. Distribution of the optical energy during propagation for a monomode and a multimode waveguide PIN photodiode structure. The multimode structure is given in Table I (structure 2) and the monomode one is the same but the GaInAsP has been replaced by InP. The spot width at $e^{-1}$ is 2 $\mu$m.

allows a quantum efficiency as high as 0.92 (0.64). This comparison shows that the multimode structure is by far the best.

*Influence of Spot Size and Position:* We continued the study by changing the illumination conditions. The quantum efficiency obtained with the monomode and the multimode structure when the spot width increases is presented in Fig. 3. The typical behavior of the monomode structure makes it very sensitive to this parameter. On the other hand the confinement of the optical energy in the multimode structure leads to a decrease of only 0.2 (0.14) of the quantum efficiency when the

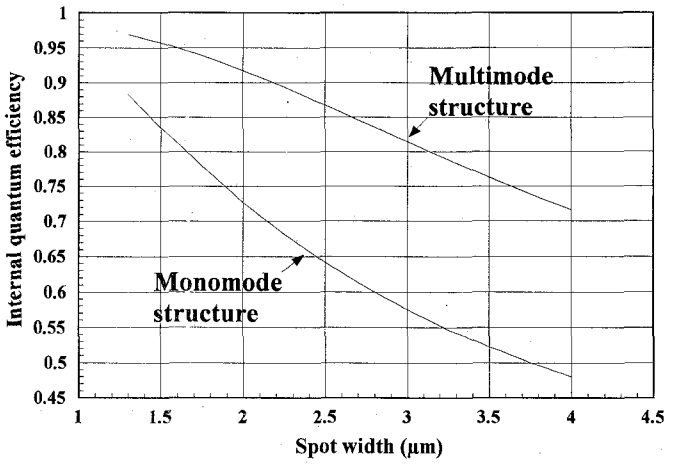


Fig. 3. Influence of the spot width on the quantum efficiency of the monomode and the multimode structure of Fig. 2.

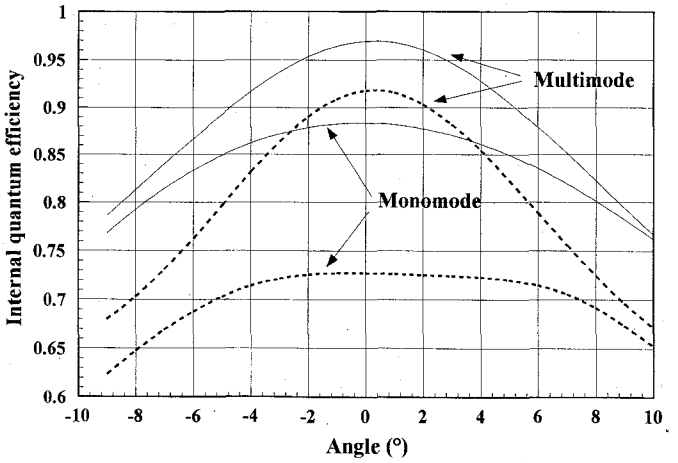


Fig. 5. Influence of the injection angle for two spot widths: continuous line: 1.3 $\mu$m, dashed line: 2 $\mu$m. The injection plan is $(X, Z)$ and when the angle increases, the light is injected toward the substrate.

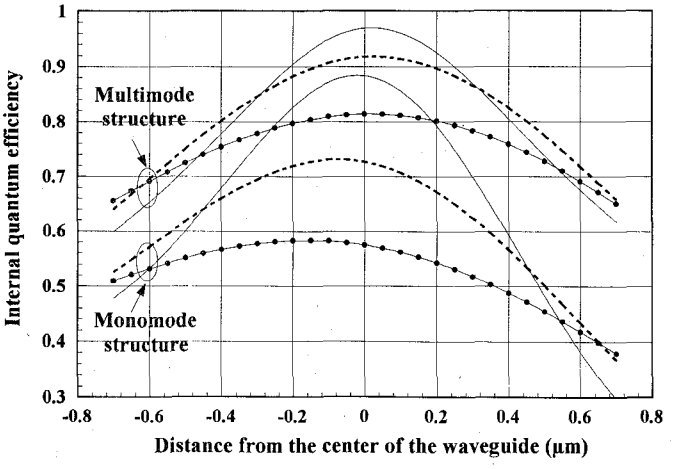


Fig. 4. Influence of the spot vertical position for different spot widths: continuous: 1.3 $\mu$m, dashed line: 2 $\mu$m, pointed line: 3 $\mu$m. When $X$ increases the light is progressively injected into the substrate.

spot width increases from 1.3 to 4 $\mu$m. The influence of the spot width and also of the spot position ($X$ direction) for the monomode and the multimode structure is presented in Fig. 4.

We finished this study with the influence of the injection angle (Fig. 5). We considered the modification of the quantum efficiency for two spot widths 1.3 and 2 $\mu$m. The multimode structure is the more sensitive to this parameter. This is due to the fact that the propagation distance where absorption occurs is smaller in the monomode structure ($\cong$4 $\mu$m) than in the multimode one ($\cong$6 $\mu$m, leading so to a smaller dependance on injection angle.

As a conclusion from this optical study, it is shown that the confinement of the multimode structures allows a higher quantum efficiency in all cases (see Figs. 3–5). The following parts of this paper are so focused on multimode structures which are listed in Table I.

*Influence of the Metallization:* Concerning now the effects of the metallization, we studied two types of ohmic contact on InP P+: the alloyed Au-Zn and Au-Be contacts and the multilayered P+GaInAs/Ti/Pt/Au contact which allows a small contact resistance [18] on InP. We simulated the following contact structure: GaInAs(2000 Å)/Ti(100 Å)/Pt(300 Å)/Au(1600 Å).

The results showed that the multimode structure is less sensitive to the influence of ohmic contact than the monomode one. This is due to the fact that this structure better confines the light. Moreover, in order to minimize contact absorption (at a value lower than 2%) in multimode structures, the thickness between the GaInAs layer of the waveguide and the contact has to be higher than 1 $\mu$m.

*Optical Behavior of the Structures Studied in this Paper:* For each structure listed in Table I, we calculated the decrease of the optical energy during propagation due to its redistribution and its absorption in the GaInAs layer. The spot width at $e^{-1}$ is 2 $\mu$m. The quantum efficiency obtained for a device length of 12 $\mu$m is 0.87, 0.92 and 0.92 (0.61, 0.64 and 0.64) respectively for the structures 1, 2 and 3. For all these structures, the quasi totality of injected light is absorbed at $Z = 6$ $\mu$m but the absorption of the thinner structure (structure 1) is more progressive. The generation rate in the absorbing layer has been calculated following this method:

—in order to use a bidimensional approach $(X, Z)$, we approximated the gaussian light distribution versus $Y$ as a constant value over a distance of the spot width $W_s$

$$\begin{aligned} -W_s/2 < Y < W_s/2 \quad & \text{Popt} = \text{cte} \\ Y > W_s/2 \quad & \text{Popt} = 0 \end{aligned}$$

—we assumed the generation rate constant with the direction $X$ in the absorbing layer

—with the direction $Z$, we have

$$G(X,Z) = -\frac{1}{h \cdot \nu} \cdot \frac{1}{W_s \cdot W_{\text{GaInAs}}} \cdot \frac{dP(Z)}{dZ}$$

where $G(X, Z)$ (cm$^{-3}$/s) is the electron or hole generation rate at $(X, Z)$, $P(Z)$ the optical power at $Z$ calculated with the BPM, and $W_{\text{GaInAs}}$ the absorbing layer thickness. The generation rate distributions obtained for the three simulated structures (Fig. 6) and for an optical input power of 1 $\mu$W allow to observe that there is a decrease of the generation

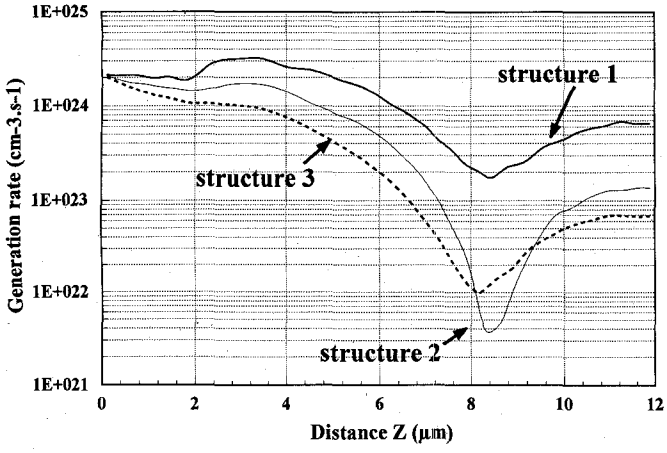


Fig. 6. Distribution of the generation rate in the structures 1, 2 and 3. The spot width is 2 $\mu$m and the input optical power is 1 $\mu$W.

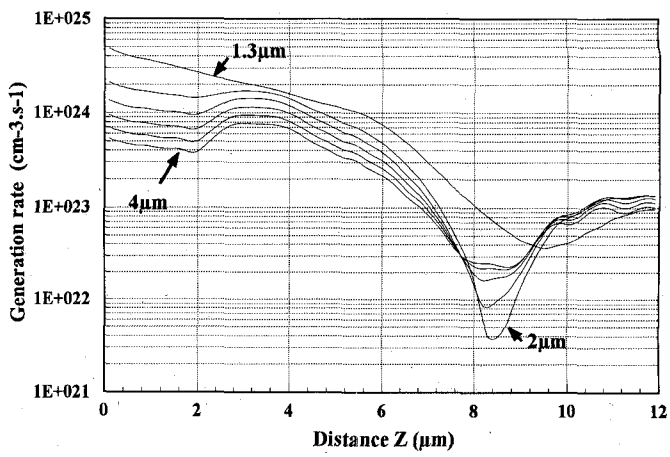


Fig. 7. Distribution of the generation rate in the structure 2 with the influence of the spot width. The spot width is successively 1.3, 2, 2.5, 3, 3.5 and 4 $\mu$m and the input optical power is 1 $\mu$W.

rate around $Z = 8$ $\mu$m due to the very small optical energy present in the absorbing layer at this place. Thus, as it can be expected, the thinner the absorbing layer is, the higher the generation rate is. As an example, for $Z = 4$ $\mu$m, we have

$$G(X, 4\ \mu\text{m})_{\text{structure 1}} \cong 2 \cdot G(X, 4\ \mu\text{m})_{\text{structure 2}} \cong 3 \cdot G(X, 4\ \mu\text{m})_{\text{structure 3}}.$$

Moreover the conditions of illumination are of great importance. The effect of different spot widths is shown in Fig. 7 for the structure 2. The comparison between the Figs. 6 and 7 permits to conclude that, concerning the behavior under high optical power, the influence of the structure and those of the illumination conditions are of the same order. This is why, in a first step, we set the spot width to 2 $\mu$m, value which can be experimentally obtained with a lensed fiber in order to present results as typical as possible for this type of photodetector. In a second step, we studied the effects of the spot size on the behavior of the structure 2 under high optical power.

### *B. Electrical Analysis*

We used a complete Drift-Diffusion model [19] coupled with an algorythm which includes the external circuit. Knowing the electrical structure of the waveguide PD (Fig. 1), we assume that there is no carrier displacement in the direction of light propagation $Z$. We neglected the transport phenomena which could occur due to the variation of generation rate versus $Z$ (see Fig. 6) which leads to the variation of carrier densities versus $Z$. So, we separated the photodetector in 10 slices (versus $Z$) where the generation rate is assumed to be constant and constituted a pseudo 2D electrical modeling. The values of conduction and valence band discontinuities at the different heterointerfaces have been taken from [16], [20] and the carrier velocities from [1], [21]. The external circuit is introduced as a relation between the total DC circuit bias voltage $V_{\text{bias}}$ and the total photocurrent $i_d$. A schematic view of the whole modeling is presented in Fig. 8. The external circuit is represented by the following equations which are solved at each time step:

$$v_d = \frac{1}{C_1} \cdot \int i_1 \cdot dt + R_1 \cdot i_1$$
$$v_d = L_2 \cdot \frac{di_2}{dt} + R_2 \cdot i_2 + V_{\text{bias}}$$
$$i_d = i_1 + i_2$$

where $i_2$ is the microwave part of the photocurrent and $i_1$ the CW part. $C_1$ and $L_2$ are the components of the bias tee allowing a good behavior at 60 GHz.

Moreover, the effects of temperature are not important in our case because the carrier densities obtained under high optical power in the absorbing layer of the photodetector do not exceed $10^{18}$ cm$^{-3}$, which has no influence on the absorption coefficient of bulk material and on the current flow in the structure.

## III. Waveguide PIN PD Behavior Under Very High Optical Modulated Power

To validate the model, we modeled the waveguide PIN PD used by Wake *et al.* [11]. Then the structures 1, 2 and 3 have been simulated in typical conditions of use. The bias voltages are 0 V and $-1$ V for structure 1, $-1$ and $-2$ V respectively for structures 2 and 3. These bias voltages are sufficiently high to obtain a good dynamic responsivity at 60 GHz in small signal conditions but not too high to avoid breakdown. The input optical signal has the following form:

$$P(t) = P_0 \cdot (1 - m \cdot \cos(2 \cdot \pi \cdot f \cdot t))$$

where $f$ is the modulation frequency and $m$ the modulation depth (in this work, $m = 1$).

For each structure, using the temporal response calculated with the model at different average optical input powers and applying the Fast Fourier Transform, we obtained the microwave response at 60 GHz.

### *A. Comparison with Experimental Results*

The structure used by Wake *et al.*, given in [22], has a 0.13-$\mu$m-thick GaInAs layer and the low doped region is 0.23 $\mu$m

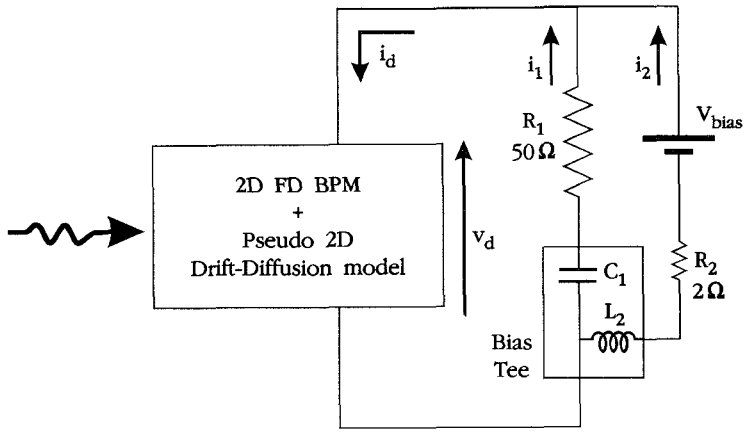


Fig. 8. Schematic view of the whole modeling.

thick. The rib width is 5 $\mu$m and the device length 10 $\mu$m. The measurements performed with a lensed fiber lead to an external quantum efficiency of 40% without AR coating. Our modeling leads to a smaller value (36%) if the spot width is around 1 $\mu$m. This difference can be explained by the fact that the real input light beam is convergent, while the beam introduced in the calculations is parallel. The modulation depth of the optical input signal is equal to 1. The microwave response of the photodetector at 30 GHz obtained with our model is compared to experimental values in Fig. 9. The simulated curve is lightly under the experimental one but they are in good agreement. The saturation phenomenon is due to the very high carrier density in the depletion region of the PD, which decreases the electric field. For higher voltage (−2 V), we obtain a breakdown around 10 mW due to the very high electric field at the GaInAsP P+/GaInAs N− heterointerface.

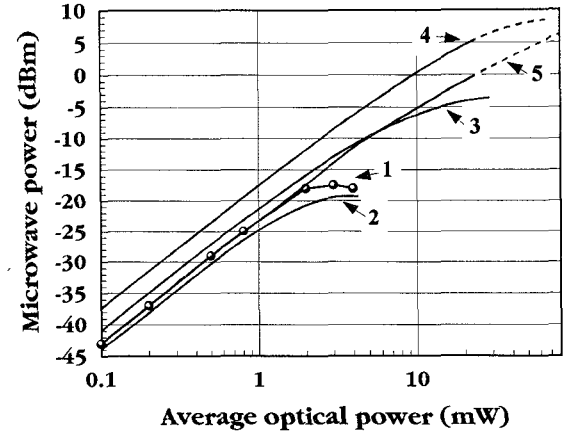


Fig. 9. Microwave responses at 60 GHz . 1) experimental results of Wake *et al.*, 2) Our results. 3) structure 1: $V_{bias} = 0$ V and $W_s = 2$ $\mu$m, 4) structure 1: $V_{bias} = -1$ V and $W_s = 2$ $\mu$m, 5) structure 3: $V_{bias} = -2$ V and $W_s = 2$ $\mu$m. The breakdown conditions are shown with dashed lines.

### *B. Behavior of the Structures 1, 2 and 3*

The calculated cut-off frequency of the structures 1, 2 and 3 is respectively 75, 68 and 56 GHz. The main interest of using a 0.6-$\mu$m photodetector whose cut-off frequency is lower than 60 GHz is its lower carrier density compared to a thinner one. The microwave responses of the three PD's at 60 GHz are presented in Figs. 9 and 10. The behavior of each photodetector under very high optical power is due to three differents phenomena

—the increase of the carrier density in the undoped absorbing layer of the PD

—the modification of the PD voltage $v_d$ due to the external circuit

these both phenomena are cumulative and lead to a decrease of the electric field in the device, which becomes too small to allow a good behavior at 60 GHz.

—the increase of the electric field at the GaInAsP P+/GaInAs N− heterointerface.

The increase of the maximum heterointerface electric field with optical power is presented in Fig. 11 for each case. The critical value of electric field in GaInAs is 200 kV/cm [23].

The structure 1 leads to saturation near 20 mW input optical power at 0 V. There is no breakdown in this case (Fig. 11) because the bias voltage is low, which demonstrates that unbiased structures are interesting. On the other hand, for a 1-V reverse bias voltage, this structure allows a higher microwave signal, due to higher electric field in the depletion region but breakdown occurs around 20-mW input optical power. As a conclusion for this structure, the maximum output microwave power which can be obtained at 60 GHz is near 5 dBm but the conditions of use are difficult because the breakdown is not far. The high sensibility to breakdown of such structures when a reverse bias voltage is applied is due to the fact that when the carrier densities are very high in the depletion region, the electric field is redistributed toward the P+/N− heterointerface, so it increases quickly with reverse applied voltage.

The structures 2 and 3 have together a similar behavior without saturation of the output microwave power but with breakdown. Their responsivity is lower than the structure 1 with −1 V reverse bias voltage due to the GaInAs thickness and the used bias voltage, but they allow respectively an output microwave power of 0 and −5 dBm without breakdown. When it occurs, it is also due to the GaInAsP P+/GaInAs N− heterointerface electric field. The microwave power which can

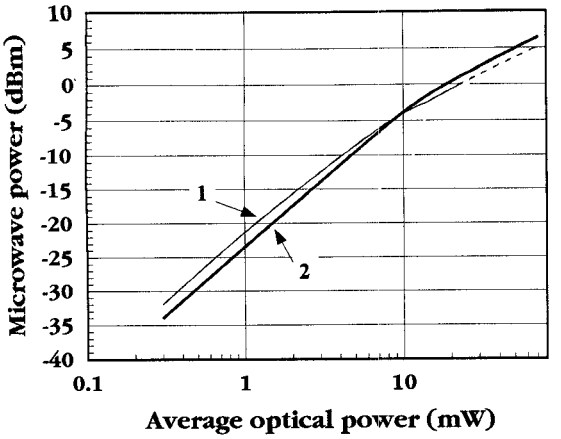


Fig. 10. Microwave responses at 60 GHz of the structure 2 ($V_{\text{bias}} = -1$ V): 1) spot width = 2 $\mu$m, 2) spot width = 4 $\mu$m. The breakdown conditions are shown with dashed lines.

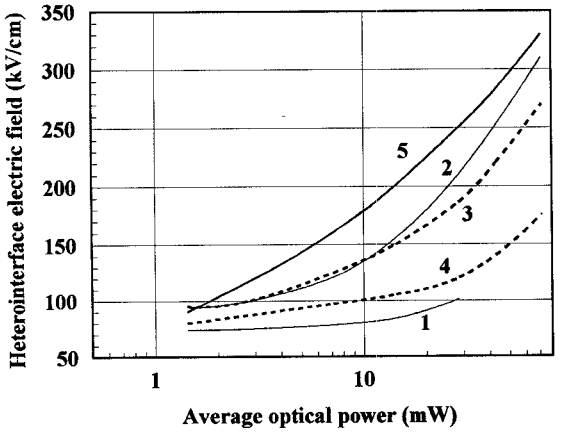


Fig. 11. Maximum electric field at the P+/N− heterointerface versus average optical power. 1) structure 1: $V_{\text{bias}} = 0$ V spot width = 2 $\mu$m, 2) structure 1: $V_{\text{bias}} = -1$ V and $W_s = 2$ $\mu$m, 3) structure 2: $V_{\text{bias}} = -1$ V and $W_s = 2$ $\mu$m, 4) structure 2: $V_{\text{bias}} = -1$ V and $W_s = 4$ $\mu$m, 5) structure 3: $V_{\text{bias}} = -2$ V and $W_s = 2$ $\mu$m.

be obtained with these two biased structures are in the same order as those obtained with the unbiased structure 1 (Figs. 9 and 10).

Considering now the effects of the spot width, the microwave responses of the structure 2 for 2 and 4 $\mu$m spot width presented in Fig. 10 (and the heterointerface electric field in Fig. 11) allow to observe that the responsivity is lower in small signal condition when the spot width is 4 $\mu$m due to the lower quantum efficiency obtained for this value, but the smaller generation rate in the structure (Fig. 7) and so, the smaller carrier density in the depletion region, allows a better microwave level under very high optical power. Moreover, for a 2 $\mu$m spot width, the breakdown occurs near an optical power of 25 mW, while it occurs theoreticaly at optical power higher than 100 mW for a 4 $\mu$m spot width. This permits to conclude that the illumination conditions are of great importance: the smaller the carrier density in the depletion region is, the higher the achievable output maximum microwave power is. As consequence, there is a compromise due to the fact that a larger spot avoids breakdown while it decreases the quantum efficiency.

## IV. Conclusion

We have presented the results of the modeling of PIN waveguide photodetectors under high optical modulated power taking into account the external circuit. At first, the optical analysis using FD BPM demonstrated the interest of the multimode structures. Because they confine the light very well, these structures are less sensitive to the different conditions of illumination: spot width, spot position and injection angle, and they allow to obtain the higher quantum efficiency in all conditions. Second we validated our modeling using experimental results presented in the literature and studied the behavior of three different waveguide PIN structures (the GaInAs absorbing layer thickness is successively 0.2, 0.4 and 0.6 $\mu$m) at 60 GHz under high modulated optical power. At first, our calculations showed the interest of thin unbiased structures: they allow as high as −5 dBm microwave output power without breakdown. Second, this study showed the interest of structures with thick absorbing layer because they allow to use larger spot size without a strong decrease of the quantum efficiency and the carrier densities in the device are lower for the same input optical power, which avoids breakdown. These structures permit to get up to 5-dBm microwave output power and the optical input power which leads to this microwave power is in the order of 50 mW.

## Acknowledgment

The authors wish to thank C. Dalle and M. R. Friscourt from I.E.M.N. for their contribution to the realization of the modeling tool and J. C. Renaud and F. Deborgies from Thomson L. C. R. for fruitfull discussions.

## References

[1] M. Dentan and B. de Cremoux, "Numerical simulation of the nonlinear response of a PIN photodiode under high illumination," *J. Lightwave Technol.*, vol. 8, pp. 1137–1144, Aug. 1990.

[2] R. D. Esman and K. J. Williams, "Measurements of harmonic distortion in microwave photodetectors," *IEEE Photon. Technol. Lett.*, vol. 2, no. 7, pp. 502–504, July 1990.

[3] K. J. Williams and R. D. Esman, "Observation of photodetector nonlinearities," *Electron. Lett.*, vol. 28, no. 8, pp. 731–733, Apr. 1992.

[4] K. J. Williams, "Nonlinear mechanisms in microwave photodetectors operated with high intrinsic region electric field," *Appl. Phys. Lett.*, vol. 65, no. 10, pp. 1219–1221, Sept. 1994.

[5] I. S. Ashour, J. Harari, J. P. Vilcot, and D. Decoster, "High optical power nonlinear dynamic response of AlInAs/GaInAs MSM photodiode," *IEEE Trans. Electron Dev.*, in press.

[6] A. F. Salem, A. W. Smith, and K. F. Brennan, "Theoretical study of the effect of an AlGaAs double heterostructure on metal-semiconductor-metal photodetector performance," *IEEE Trans. Elect. Devices*, vol. 41, no. 7, pp. 1112–1119, July 1994.

[7] K. Kato, S. Hata, K. Kawano, J. Yoshida, and A. Kozen, "A high efficiency 50 GHz InGaAs multimode waveguide photodetector," *IEEE J. Quantum. Electron.*, vol. 28, no. 12, pp. 2728–2735, Dec. 1992.

[8] R. R. Hayes and D. L. Persechini, "Nonlinearity of PIN photodetectors," *IEEE Photon. Technol. Lett.*, vol. 5, no. 1, pp. 70–72, Jan. 1993.

[9] A. R. Williams, A. L. Kellner, A. L. Jiang, and P. K. L. Yu, "InGaAs/InP waveguide photodetector with high saturation intensity," *Electron. Lett.*, vol. 28, no. 24, pp. 2258–2259, Nov. 1992.

[10] A. R. Williams, A. L. Kellner, and P. K. L. Yu, "High frequency saturation measurements of an InGaAs/InP waveguide photodetector," *Electron. Lett.*, vol. 29, no. 14, pp. 1298–1299, July 1993.

[11] D. Wake, N. G. Walker, and I. C. Smith, "Zero-bias edge coupled InGaAs photodiodes in millimeter wave radio fiber systems," *Electron. Lett.*, vol. 29, no. 21, pp. 1879–1881, Oct. 1993.

[12] R. P. Ratowsky, J. A. Fleck, and M. D. Feit, "Helmholtz beam propagation in rib waveguides and couplers by iterative Lanzcos reduction," *J. Opt. Soc. Am. A.*, vol. 9, no. 2, pp. 265–273, Feb. 1992.
[13] P. Kaczmarski and P. E. Lagasse, "Bidirectional Beam Propagation Method," *Electron. Lett.*, vol. 24, no. 11, pp. 675–676, May 1988.
[14] Y. Chung and N. Dagli, "An assessment of finite difference beam propagation method," *IEEE J. Quantum Electron.*, vol. 26, no. 8, pp. 1335–1339, Aug. 1990.
[15] K. Kato and J. Yoshida, "Ultrawide bandwidth 1.55 $\mu$m waveguide PIN photodiode," *Proc. SPIE*, Los Angeles, vol. 2149, pp. 312–319, Jan. 1994.
[16] T. P. Pearsall, *GaInAsP Alloy Semiconductors*. New York: Wiley, 1982.
[17] *CRC Handbook of Chemistry and Physics*, 64th edition, 1988–89.
[18] A. Katz, Ed. *Indium Phosphide and Related Materials: Processing, Technology and Devices*. Norwood, MA: Artech House, 1992.
[19] C. Dalle and P. A. Rolland, "Drift-Diffusion versus energy model for millimeter wave IMPATT diodes modeling," *Int. J. Numerical Modeling: Electron. Networks, Devices and Fields*, vol. 2 pp. 61–73, 1989.
[20] S. R. Forrest, P. H. Schmidt, R. B. Wilson, and L. Kaplan, "Relationship between the conduction band discontinuities and bandgap differences in InGaAsP/InP heterojunctions," *Appl. Phys. Lett.*, vol. 45, p. 1199, 1984.
[21] P. Hill, J. Schlafer, W. Powazinik, M. Urban, E. Eichen, and R. Olshansky, "Measurements of hole velocity in N-type GaInAs," *Appl. Phys. Lett.*, vol. 50, no. 18, pp. 1260–1262, May 1987.
[22] D. Wake, T. P. Spooner, S. D. Perrin, and J. D. Henning, "50 GHz InGaAs edge coupled PIN photodetector," *Electron. Lett.*, vol. 27, no. 12, pp. 1073–1075, June 1991.
[23] J. Harari, D. Decoster, J. P. Vilcot, B. Kramer, C. Oguey, P. Salzac, and G. Ripoche, "Numerical simulation of avalanche photodiodes with guard ring," *IEE Proc.*, pt. J, vol. 138, no. 3, pp. 211–217, June 1991.

**Joseph Harari** was born in Enghien, France, in 1961. He received the engineer degree from Polytechnic Institute of Grenoble in 1985 and Ph.D. degree from the University of Lille in 1991 where his work dealt with avalanche photodiode modeling. He joined the IEMN, Département Hyperfréquences et Semicon-ducteurs, in 1992.

He is currently Assistant Professor at the Engineering School of the University of Lille (Ecole Universitaire D'Ingénieurs de Lille: EUDIL). His current activities focus on the simulation of optoelectronic devices for mm-wave applications and integrated optics.

**Frédéric Journet** was born in Fourmies, France, in 1967. He received the Ms.D degree in electronics from the University of Lille in 1992. Since 1993, he has been preparing a Ph.D. thesis in electronics at IEMN. His work deals with the modeling of long-wavelength photodetectors for microwave applications.

**Omar Rabii** was born in Meknés, Morocco, in 1966. He received the Ms.D degree in physics from the University of Rabat in 1990. Since 1991, he has been preparing a Ph.D. thesis in electronics at IEMN. His work deals with the modeling of waveguide-type photodetectors for microwave applications and integrated optics.

**Guanghai Jin** was born in Harbin, China, in 1960. He received the Bs. and Ms. degrees in applied physics from Harbin Institute of Technology in 1982 and 1984, respectively. He joined the IEMN in 1994 for the Ph.D.

From 1984 until 1994, he worked as Assistant Professor at Harbin Institute of Technology. His research activities dealt with integrated optics on $LiNbO_3$. His primary interests are on integrated optoelectronic devices and also on integrated optics.

**Jean Pierre Vilcot** was born in Lens, France, in 1958. He received the Ph.D. degree in electronic from the University of Lille, France, in 1984, where his work dealt with III–V photoconductors.

Between 1984–86, he worked as a Microwave Engineer, mainly in the field of X-band satellite receivers. He joined the Centre Hyperfréquences et Semiconducteurs (now IEMN, Département Hyperfréquences et Semiconducteurs) in 1986 as a Scientist of the Centre National de la Recherche Scientifique (CNRS). His current activities include photonic and optoelectronic integrated circuits, microwave-optical interactions and optical interconnection.

**Didier Decoster** was born in Lille, France, in 1948. He received the Ph.D. degree in electronics and physical science (Doctorat d'Etat) at the University of Lille.

He is currently a Professor at the Engineering School of the University of Lille (Ecole Universitaire D'Ingénieurs de Lille: EUDIL), in the Material Science Department. His research activities are with the Institut d'Electronique et de Microélectronique du Nord (IEMN), where he is the leader for the electromagnetism, optoelectronics and opto-acoustics group. His own activities include optoelectronic and photonic components and integrated circuits on III–V materials, microwave applications of optics, and optical interconnection.